Supplementary Materials

David Reens,* Hao Wu,* Tim Langen,† and Jun Ye
JILA, National Institute of Standards and Technology and the University of Colorado and Department of Physics, University of Colorado, Boulder, Colorado 80309-0440, USA
(Dated: September 26, 2017)

The present study on the role of mixed fields for spin-flip loss evolved out of our continuing investigations into the collisional processes reported in Refs. [1, 2]. These investigations have revealed that an important fraction of the effects previously attributed to collisions are in fact attributable to spin-flip losses. In Secs. A, B we provide the interested reader with our current best understanding of the situation. Lastly, we provide in Sec. C an algebraic derivation of the loss enhancement factor presented in Eqn. 3 of the main text [3].

A. Electric Field Induced Collisions

We begin with Ref. [1] on electric field induced inelastic collisions. The authors identified the same single particle spin-flip loss enhancement process we discuss [3], and an attempt was made at deconvolution from the collisional effect (App. A, Ref. [1]). Since that time, new experimental observations have prompted important improvements to the analysis that was presented there.

Relative to the approach taken in App. A of Ref. [1], we make the same simplifying assumptions: loss only occurs in the $\vec{E} \perp \vec{B}$ plane, only the velocity orthogonal to this plane matters, and the population is a thermalized Maxwell-Boltzmann distribution. Our improvement relates to the next step, where an integral calculation for the loss rate is performed. In Ref. [1] the integration spans the entire 3D spatial distribution, weighted by the frequency of crossing of the center plane and the chance of loss for each crossing:

$$\Gamma_{\mathrm{LZ}} = \int_0^\infty 4\pi r^2\, n(r) dr \int_0^\infty n(v_\theta) dv_\theta \left(\frac{v_\theta}{\pi r} P_{\mathrm{hop}}(r, v_\theta)\right) \quad (1)$$

Here $n(r)$ is the radial distribution function, constrained to satisfy $\int_0^\infty 4\pi r^2 n(r) = 1$, and of the form $n(r) \propto e^{-\mu_B B' r/kT}$. Likewise $n(v_\theta)$ is the usual normalized Maxwellian velocity distribution. Implicit in this integration is the assumption that molecules at a given radius r cross the center plane with a frequency of $v_\theta/\pi r$. This approximation is rather rough given that molecules are typically not following circular orbits of constant v_θ but are in general following some complex trap motion. Our improvement is to perform an integration of flux through the loss plane directly:

$$\Gamma_{\mathrm{LZ}} = \int_0^\infty 2\pi r\, n(r) dr \int_0^\infty n(v_z) dv_z \left(v_z P_{\mathrm{hop}}(r, v_z)\right) \quad (2)$$

Here the same distributions are used, but the spatial is integrated over the central plane only, hence the $2\pi r$ Jacobean, and the hopping probability is multiplied by v_z to give a flux. We change to cylindrical coordinates to highlight our focus on the central plane. This flux integral gives the desired loss rate without any approximations about molecule orbits or plane-crossing frequency. Although the two integrals differ significantly in conception, mathematically the differences reduce to precisely an overall scaling factor of π.

The influence of this on the deconvolution procedure relates to the details of the two-body fitting routine. One plus two body fits $\dot{N} = -\gamma N - \beta N^2$ were performed to various decay trap curves, with the one body rate γ fixed to the value expected due to vacuum scattering and spin-flip loss. An example of such decay curves is shown in Fig. S1, where electric field is turned on suddenly after various hold times. With the stronger spin-flip loss, it is no longer appropriate to assume this loss will be present in the data as a pure one-body decay. Rather, only those molecules whose orbits regularly intersect the loss region are lost, after which thermalization would be required to repopulate the loss prone trajectories of phase space.

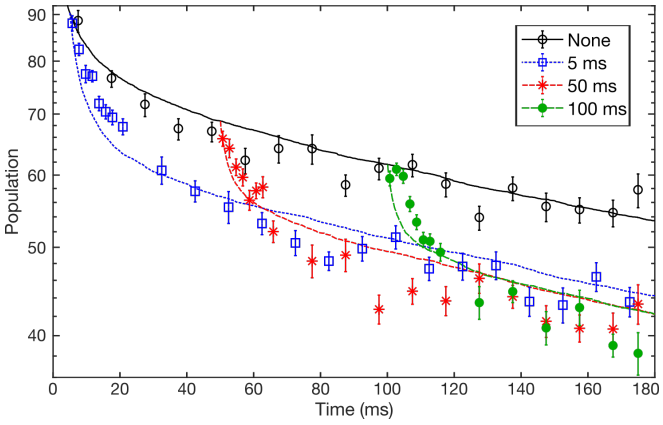

FIG. S1. Experimental electric field induced loss data with an attempted overlap to spin-flip loss simulations. The case of no electric field (black, solid, circles) is compared to electric fields of 3 kV/cm turned on after a wait time indicated in the legend.

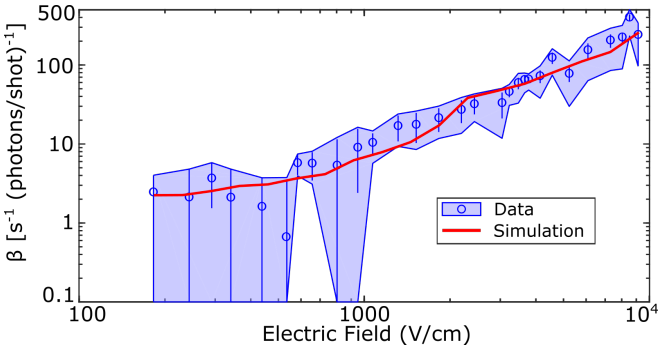

FIG. S2. Two body fits from [1] to experimental data like that in Fig. S1 but at various electric fields. The blue data points and shaded region are repeated from Fig. 3 of [1], where the shading indicates the variation that would be brought about by two-fold changes in γ from spin-flip losses. Even though we discover a factor of only three, the spin flip loss simulation (thick red line) matches the data within errorbars.

If thermalization is slow, spin-flip loss can have a rate that decreases over time, producing a time dependence of population like that of a two-body effect. Even though the possibility of a factor of two error in the calculated magnitude of spin-flip loss was considered in Ref. [1] (Repeated here in Fig. S2, shaded regions), the possibility of its influencing the data in a non-single-particle manner was not addressed.

We can perform single particle Monte Carlo simulations of spin-flip loss to investigate this, and we obtain curves such as shown above the experimental data in Fig. S1. We can even perform the same one plus two body fitting procedure to the single particle spin-flip loss simulation traces. The single particle traces yield "two-body" values that overlap nicely with those derived in Ref. [1], see Fig. S2. This suggests that the effect attributed to two-body collisions is largely explained by spin-flip losses. Still, there are notable discrepancies, such as in the initial rate of the decays in Fig. S1. One avenue to try and improve agreement would be to incorporate collisions in the simulation. Unfortunately there are many challenges in the quantitative application of these simulations, such as the existence of various partially trapped substates. We think the best path forward is to perform future collisional studies with the single-particle effect removed, as achieved in our most recent trap [3].

B. Evaporation

With regard to Ref. [2], the present study has important ramifications. The process of evaporation and of depletion spectroscopy both require two steps. First molecules are transferred from positive to negative parity by microwaves targeting a specific range of magnetic fields. After this transfer, the molecules are still trapped, and only by the subsequent addition of electric field to open avoided crossings can these opposite parity molecules escape from the trap. In the case of depletion spectroscopy, there is a final step of measuring the population by laser induced fluorescence, so that the population originally at the magnetic field transferred by microwaves can be inferred by subtraction. The crossings opened by electric field would only allow molecules in the upper 90% of the trap to escape, so it was thought that a cold population insensitive to the spectroscopic technique could be building up at low magnetic fields. Given the existence of spin-flip loss caused by the electric field at the very center of the trap where such a cold population would build up, and given its strength for the relevant temperatures and electric fields (Tab. I of the main text [3]), we reject this hypothesis.

Without the cold hidden population hypothesis, the temperature fits performed in Fig. 3 of Ref. [2] are significantly altered, and only panels (a-c) can be reasonably fit. Nonetheless, the normalized spectra can still be used to identify enhancements in density caused by the evaporation. Since the publication of Ref. [2], we have repeatably found such enhancements for evaporation sequences designed to achieve a twofold temperature reduction, see Fig. S3. The initial temperature of 59 ± 2 mK is higher than reported in Ref. [2] due to an important correction to the molecular Hamiltonian found by inclusion of nearly one hundred ground and excited hyperfine levels [4].

Regarding the normalization procedure, the idea is to require the area beneath the curve to add up to the observed total population by laser induced fluorescence. This is necessary because the spectroscopy is performed over a total time of about a quarter of a trap oscillation, so that molecules are not at all frozen in place. Relative to a very brief spectroscopy pulse that would only deplete molecules in a given region at that particular instant, the longer pulse can be seen as a way of boosting the signal to noise ratio of the experiment. The spectroscopy still gives a value that ought to be proportional to the true instantaneous population in the region of interest, but with a scaling factor relating to details of population transfer in and out of the region of interest while it is probed. Without normalization, spectroscopies of smaller total populations yield distributions with enclosed areas that are decreased much more than the actual population. In the future, a variety of density enhancing strategies [3] may improve our signal enough that a more straightforward spectroscopy could be performed without the need for normalization. For the time being, we find no particular reason to distrust the normalization procedure, and we carefully include all of the steps in the error analysis leading to the error bars shown in Fig. S3.

Seeking more direct and sensitive verification of the collisional effect, we have compared the populations under two related treatments. The first is a normal evaporation sequence and the second is identical but with a

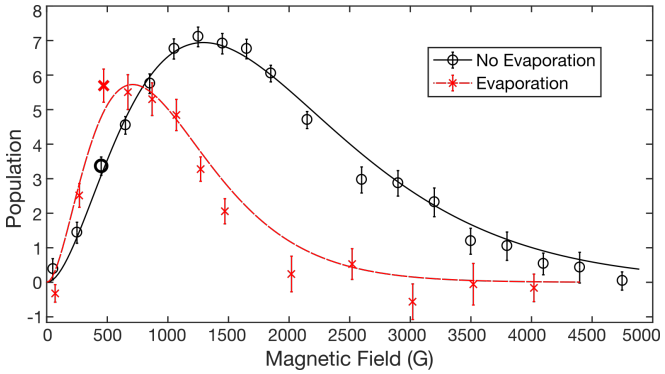

FIG. S3. Normalized spectra are performed after evaporation (red x's) and without evaporation (black circles). Solid lines are fits to Maxwell-Boltzmann distributions with temperatures of 59 ± 2 without evaporation (black), and 30 ± 3 for evaporation (red, dashed). The evaporation achieves a clear density enhancement in the vicinity of 500 G, where the line markers are bolded.

time-reversed microwave frequency chirp, so that the cut goes backwards from deep to shallow. This comparison subjects all molecules to the same integrated microwave power, and thus the two conditions should be equivalent in a situation with only single particle effects. With respect to collisional effects, the time-reversed case functions like a truncation, preventing molecules that would otherwise have collisionally thermalized to lower temperatures from doing so. To whatever extent an evaporation is successful in facilitating beneficial thermalizing collisions, the time-reversed condition should yield fewer molecules. We consistently observe this at the $(6 \pm 2)\%$ level, suggesting a slight evaporative effect despite the negative influence of spin-flip losses.

We have also developed the ability to reduce the size of the population without perturbing its phase space distribution, utilized in our new trap as described in the main text [3]. This ought to reduce the influence of collisional processes, but keep any single particle effects the same, thus disambiguating the two. Many possible approaches have key drawbacks, for example changing the partial pressure of water in our supersonic expansion would require changing the temperature of the valve and thereby influencing the initial speed of the beam. We opt for the application of microwaves during deceleration, leading to a probability for transitioning from a weak to strong field seeking state and being deflected out of the beam. We tune the microwaves to be resonant only at low magnitudes of electric fields, experienced by all molecules when flying through a de-energized stage just after switching. The microwaves are applied via microwave horn and have a long wavelength relative to the cloud, so that microwave power variations across the cloud are minimal. The microwaves are applied early during deceleration, so that the molecules have many stages of deceleration left to remix any outstanding asymmetries in the removal process. It is difficult to experimentally verify that the phase space distribution is truly unaffected, but in at least one projection of phase space, the time of flight profile of slowed molecules after deceleration, the distribution is unaffected even by tenfold reductions using this technique.

In conclusion, the role of collisional effects in Ref. [2] is reduced by spin-flip losses, but spectroscopic comparisons and evaporation subtractions still suggest an evaporative effect. The development of forward to backward comparisons and homogeneous density reductions has us poised to more unambiguously identify any future collisional effects in our next generation system.

C. Scaling Law Derivation

Here we derive the loss enhancement scaling law presented in Eqn. 3 of the main text [3], and repeated here:

$$\eta \propto \left(\frac{d_{\text{eff}} E}{\sqrt{\kappa \Delta}} \right)^{8/3}. \tag{3}$$

The key idea is to compare the surface areas of the loss regions with and without electric field. There is no exact loss region where a molecule is guaranteed to hop, but rather its velocity and direction contribute to the Landau-Zener probability (Eqn. 2, Ref. [3]). Nonetheless, for the purposes of a scaling law, we can assume the average thermal velocity v_T, and choose a probability threshold of $P > 1/e$. These assumptions allow us to define the loss region as the contour surface of energy κ where

$$\kappa = \sqrt{\hbar \dot{G}} = \sqrt{2 \hbar v_T B'}. \tag{4}$$

Here G is the energy gap between the trapped state and its spin flip partner, and B' is the trap gradient along the strong axis.

We assume that the electric field is applied parallel to the strong axis of the quadrupole trap, which makes the loss plane where $\vec{E} \perp \vec{B}$ perpendicular to this axis. This matches the geometry that has been realized in our experiment [1], and is the worst case, but by no more than a constant factor of $2\sqrt{2}$ relative to other directions the electric field could have.

Before application of electric field, the κ valued energy contour is the surface of an oblate ellipsoid of long radius $r_0 = 2\kappa / \mu_{\text{eff}} B'$. Its area is then $2\pi \cdot 1.38\, r_0^2$, where the numeric factor relates to the specific $2:1$ aspect ratio of the ellipsoid and is hereafter neglected. When electric field is applied, the energy gap near the trap zero takes an unusual functional form. To derive it, we first assign spatial coordinates r and z denoting directions within and normal to the loss plane, respectively. Next we diagonalize the ground state hamiltonian of OH in mixed fields, see

App. A of Ref. [5], or similarly for another species. Subtracting the energies of the trapped state and its spin-flip partner and series expanding the result then yields:

$$G = \mu_{\text{eff}} B'|z| + \alpha(\frac{1}{2}\mu_{\text{eff}} B' r)^3 \frac{\Delta\sqrt{\beta\Delta^2 + d_{\text{eff}}^2 E^2}}{(d_{\text{eff}} E)^4}, \quad (5)$$

plus higher order terms in r and z. The constants α and β are nearly unity for OH and will be ignored henceforth. The key feature, as discussed in the main text [3], is the cubic dependence G exhibits on r which leads to a much more severely oblate contours.

Now we can use Eqn. 5 to compute the surface area of the $G = \kappa$ contour. We specialize to the regime where $d_{\text{eff}} E < \Delta$, so that $\Delta \approx \sqrt{\Delta^2 + d_{\text{eff}}^2 E^2}$. The radial extent of the surface can be solved by inverting $\kappa = G|_{z=0}$:

$$r_E = \frac{1}{\mu_{\text{eff}} B'} \sqrt[3]{\frac{8\kappa(d_{\text{eff}} E)^4}{\Delta^2}}. \quad (6)$$

The axial extent remains $z = \kappa/\mu_{\text{eff}} B'$ for all $\vec{E}$. For large enough E, r_E dominates over this axial extent, so that the area is effectively $2\pi r_E^2$ and the loss area enhancement becomes $\eta = (r_E/r_0)^2$. Comparing the expressions for r_E and r_0, $\mu_{\text{eff}} B'$ cancels and we have

$$\eta = \left(\frac{1}{2\kappa}\sqrt[3]{\frac{8\kappa(d_{\text{eff}} E)^4}{\Delta^2}}\right)^2 = \left(\frac{d_{\text{eff}} E}{\sqrt{\kappa\Delta}}\right)^{8/3}. \quad (7)$$

Now we address the domain of validity of this result. When E is small, Eqn. 5 only has a narrow range of validity, since the electric field only dominates in a very small region near the trap center. Outside, G retains a nearly linear dependence on r. This means that Eqn. 6 only holds for E above some threshold. For smaller E, r_E will simply not be significantly perturbed from its zero electric field value of $r_0 = 2\kappa/\mu_{\text{eff}} B'$. The implication for the enhancement factor in Eqn. 7 is simply that it is only valid when it predicts an enhancement significantly greater than unity. In other words, Eqn. 7 holds when $d_{\text{eff}} E > \sqrt{\kappa\Delta}$, but below this η gradually returns to unity. Eventually when $d_{\text{eff}} E > \Delta$, the factor of $\sqrt{\beta\Delta^2 + d_{\text{eff}}^2 E^2}$ in Eqn. 5 is better approximated by $d_{\text{eff}} E$, which leads to the modification $\eta \propto (d_{\text{eff}} E)^2/\kappa^{4/3}\Delta^{2/3}$. Thus for these larger E-fields, the enhancement factor reduces in its dependence on electric field from order 8/3 to order 2. At this point, the loss is typically so large as to preclude all but the briefest trapping experiments, see Tab. I of the main text [3].

* Contributed equally. Email dave.reens@colorado.edu or hao.wu@colorado.edu.

† Present Address: 5. Physikalisches Institut and Center for Integrated Quantum Science and Technology (IQST), Universität Stuttgart, Pfaffenwaldring 57, 70569 Stuttgart, Germany

[1] B. K. Stuhl, M. Yeo, M. T. Hummon, and J. Ye, Molecular Physics **111**, 1798 (2013).

[2] B. K. Stuhl, M. T. Hummon, M. Yeo, G. Quéméner, J. L. Bohn, and J. Ye, Nature **492**, 396 (2012).

[3] See Main Text.

[4] K. Maeda, M. L. Wall, and L. D. Carr, New Journal of Physics **17**, 45014 (2015).

[5] B. K. Stuhl, M. Yeo, B. C. Sawyer, M. T. Hummon, and J. Ye, Physical Review A **85**, 033427 (2012).